Experimental study on Eccentric Compressive Behaviors of 6061-T6 Aluminum Tubular Long Columns Filled with Concrete

Qixuan Mi[1], Qianjin Shu[1*], Fangying Wang[2], Peixiang Liu[3], Mingquan Zhu[1], Wei Wang[1]

[1]State Key Laboratory for Geomechanics & Deep Underground Engineering, School of Mechanics & Civil Engineering, China University of Mining & Technology, Xuzhou, Jiangsu, China

[2]Department of Civil Engineering, University of Nottingham, Nottingham, United Kingdom

[3]Architectural Design and Research Institute of Tsinghua University Co., Ltd., Beijing, China

Abstract: In this paper, eccentric compressive experiments of 12 circular and 6 square concrete-filled 6061-T6 aluminum tubular (CFAT) long columns were carried out. The influence of the section forms, thickness of aluminum tubes, slenderness ratios, and eccentricity on the flexural performance of CFAT long columns was investigated. The results showed that all the specimens exhibited flexural-dominated failure. The variation of eccentricity has little impact on the aluminum tube's overall failure mode, while it dramatically influences the failure mode of the internal concrete. The internal concrete failed in concrete crushing for all square columns, while it remained intact for the circular columns. This shows that circular tubes provide a better constraint effect on the internal concrete and thus increase the ultimate strain of concrete under compression. It was also found that the increase of eccentricity leads to the weakening of the confinement effect of the aluminum tube on internal concrete, while the increase of slenderness ratio has no obvious effect on the restraining effect. Finally, the applicability of current design provisions for concrete-filled steel tubular (CFST) long columns to CFAT long columns was evaluated, and some corresponding calculation suggestions were proposed.

Keywords: Concrete-filled aluminum tube (CFAT); Eccentric compression; Long column; Bearing capacity; Lateral confinement effect; Calculation suggestion

1 Introduction

In the past 100 years, aluminum alloy sections, members and composite members made of aluminum alloy have been widely used in bridge structures, long-span buildings and aerospace engineering because of the simplicity of component manufacturing, good corrosion resistance and especially the environment-friendly characteristic due to its much higher recycling rate than steel [1, 2]. Recently, concrete-filled aluminum tubular (CFAT) columns have attracted research attention. The advantages of aluminum alloys for lighter weight, higher durability, and corrosion resistance make the CFAT members well-suited to applications in aggressive and demanding environments, such as marine and offshore engineering and so on. The present study focuses on the flexural resistance and design of CFAT long columns under eccentric loading.

In recent years, many studies have been carried out on the behaviors of CFST long columns, including the failure characters, bearing capacity, stiffness and flexibility, based on which the design guidance of CFST long members has been developed [3]. Specifically, Cederwall et al. [4] performed an eccentric compression experiment on square CFST long columns, and they found that the steel tube yields at the area of compression when the mean stress reaches 30% of the axial compressive strength of specimens. Zeghich et al. [5] found that the decline range of the stability coefficient of specimens with higher concrete strength was extensive, and the restraint effect of steel tube on internal concrete decreases with the increase of slenderness ratio. Portolés et al. [6] studied the eccentric compressive behaviors of circular CFST long columns

respectively filled with normal-strength concrete and high-strength concrete, and they found that the constraint effect of steel tube on internal concrete decreases with increasing eccentricity. Ellobody et al. [7] proved that EC4 [8] yielded acceptable accuracies in the assessment of bearing capacities of axial compressive CFST columns, by comparing theoretical results based on EC4 with test results. Yan et al. [9] found that the buckling of the steel tube was firstly caused by the crushing of internal concrete rather than the overstress of the steel tube. Gopal et al. [10] tested the eccentric compression behaviors of slender circular CFST columns respectively filled with ordinary concrete and fiber-reinforced concrete, and they found that the latter has a better contribution to the performance, especially the bearing capacities, of slender CFST columns. Portolés et al. [11] found that long circular CFST columns filled with high-strength concrete show better ductility than those filled with normal-strength concrete based on eccentric compression tests, while little increase of bearing capacity was measured. U. M. et al. [12] performed some experiments of CFDST columns (double-skinned steel tubes filled with concrete), CFST columns (steel tubes filled with concrete) and CFHSST columns (hollow single-skinned steel tubes filled with concrete), and they found that the contribution ratios of the inner tube to the bearing capacities of specimens are littler than the predicted values based on the methods respectively proposed by Han et al. [13] and Romero et al. [14]. Ouyang et al. [15] proposed a method to promote the accuracy of the FEA models of CFST specimens under eccentric compression by introducing the transverse strain-axial strain relationship of the inner confined concrete, which was validated by the test results of 95 CFST specimens presented in Literatures [5,6,16-19]. Li et al. [20] proposed a predictive equation of the bearing capacities of square high-strength steel tubular long columns filled with high-strength concrete under

eccentric compression based on test results. In general, the existing research results show that slenderness ratio, eccentricity and section shape have a great impact on the failure mode, bearing capacity, stiffness and ductility of steel tubular long columns filled with concrete.

With the development of various materials, some high-performance materials can also play the role of constraint like steel tubes, such as stainless steel, aluminum alloy, carbon fiber, etc. Uy et al. [21] studied the mechanical behaviors of CFSST (stainless-steel tube filled with concrete) stub columns under compression and also CFSST long columns under axial force together with bending moment, and they found CFSST columns have great structural performance. Similar observations were also found in previous studies on CFSST columns [22,23]. Al-Mekhlafi et al. [24] found that wrapping CFRP can obviously improve the bearing capacities of CFRP-CFSST specimens subjected to eccentric load based on experiments and simulations. He et al. [25] studied the mechanical behaviors (including failure modes, ultimate loads, transverse deflections, and load-deformation curves) of stainless-steel tubular columns, based on experiments and simulations. Cao et al. [26] investigated the influence of the thickness of the stainless-steel tube, relative eccentricity, and slenderness ratio on the compressive behaviors of rectangular CFSST columns by FEA modeling, and they found that the load-displacement curves of the columns are obviously influenced by the slenderness ratio and also relative eccentricity.

Recently, some investigations of aluminum alloy tube filled with concrete (CFAT) have been finished. An earlier investigation was carried out by Li et al. [27] on a circular compressive aluminum alloy tube, and the calculation formula of the stability coefficient was obtained. Guo et al. [28] tested the performance of 6061-T6 aluminum alloy members with different section

forms (H-shaped, T-shaped, circular and square tubes) under eccentric compression, and they proposed a formula to calculate the stability coefficient. Zhou et al. [29, 30] finished some compression tests on circular and square CFAT stub columns, and they found that the square specimens were all damaged at the corner of the aluminum tube. It was also found that the aluminum tubes with a width-thickness ratio larger than 24 showed local buckling failure and the specimens with circular sections show higher ductility than the specimens with square sections. Li et al. [31] investigated the bearing capacities of axial compressive CFAT long columns, and they found that DBJ/T13-51-2010 [32] and GB 50936-2014 [33] provide better predictions of the specimens' bearing capacities than EC4 [8], owing to the latter's neglect of the confinement effect of the aluminum tube on internal concrete. Ding et al. [34] numerically investigated the confinement effect of concrete-filled circular aluminum alloy tubular (CFCAT) stub columns, and the numerical results revealed that higher aluminum alloy strength and ratio resulted in a better confinement effect and weaker enhancement effect. Until now, no experiments or numerical studies have been carried out on the behaviors of CFAT long columns, which is the focus of current research.

Recently, increasing attention has been paid to using aluminum alloy in composite columns [29,30]. Aluminum alloys present distinct merits when compared to conventional steel. Noteworthy advantages encompass heightened corrosion resistance within atmospheric settings, obviating the need for anti-corrosion coatings. Meanwhile, aluminum alloys demonstrate resilience against brittleness at low temperatures. The combined advantages would allow the aluminum composite columns to be potentially suitable for applications in demanding environments, such as marine and offshore sectors, and exceedingly cold surroundings.

In this paper, an experimental program to investigate the behaviors of CFAT long columns under eccentric compression is presented. A laboratory testing program, comprising 12 circular columns and 6 square columns, was conducted to investigate the influence of key parameters (section types, tube thickness, slenderness ratios, eccentricity) on the flexural performance of CFAT long columns. The applicability of current design provisions given in the Eurocode EN 1994-1-1 (EC4) [8] and two Chinese design provisions GB 50936-2014 [33] and CECS 28:2012 [35] to the investigated CFAT section designs was then evaluated based on experimental data. Finally, some calculation suggestions for eccentric compressive CFAT long columns were proposed.

2 Test Design and Implementation

2.1 Preparation of test specimens

In this experimental program, 12 circular and 6 square CFAT long columns were fabricated. For all the circular CFAT columns, the nominal outer diameters of outer aluminum tubes are 160 mm while the nominal thicknesses varied (3 mm and 10 mm) to achieve distinct local slenderness ratios. The nominal width (depth) of the square aluminum tubes is 160 mm, and the nominal thickness is 6.3 mm. The ratios of length to diameter (L/D) of columns are 8 or 12. The detailed geometric dimensions of all specimens are listed in Table 1. In Table 1, R3 and R10 represent circular tube with a thickness of 3 mm and 10 mm respectively, while S6.3 represents square tube with a thickness of 6.3 mm. D represents the diameter of a circular column or the width (depth) of a square column. L, t and e respectively represent the length, tube thickness and load eccentricity of a CFAT column. α indicates the aluminum ratio, equal to the value of A_a/A_c. Here, A_a and A_c are the section areas of aluminum tube and concrete column respectively.

λ represents the slenderness ratio, taken as $4L/D$ and $2\sqrt{3}\,L/B$ respectively for circular and square CFAT columns.

A tagging system was designed for the investigated CFAT specimens in order to directly identify the CFAT cross-sectional components. For example, CFAT-R3-L8-20 defines a CFAT specimen, with the term “R3” referring to circular tubes with a thickness of 3 mm and “L8” representing length-diameter ratio (*L/D*) of 8, as well as the last number “20” standing for a load eccentricity of 20 mm.

Table 1 Serial numbers and parameters of all specimens

Serial numbers	D	t	A_a	A_c	α (%)	L	L/D	λ	e	N_u	Failure Mode	Material properties of AA		
	(mm)	(mm)	(mm^2)	(mm^2)		(mm)			(mm)	(kN)		$f_{0.2}(Mpa)$	$f_u(Mpa)$	$E_0(Mpa)$
CFAT-R3-L8-20	159.93	3.12	1537.02	18551.58	8.29		8.00	32.01	20	716.6				
CFAT-R3-L8-40	159.73	3.18	1563.98	18474.41	8.47	1280	8.01	32.05	40	527.5	1	244.55	296.89	69566
CFAT-R3-L8-60	159.91	3.05	1503.01	18580.57	8.09		8.00	32.02	60	415.4				
CFAT-R3-L12-20	160.24	3.10	1530.38	18636.18	8.21		11.98	47.93	20	652.0				
CFAT-R3-L12-40	159.89	3.15	1551.10	18527.45	8.37	1920	12.01	48.03	40	450.8	1	244.55	296.89	69566
CFAT-R3-L12-60	159.81	3.07	1511.71	18546.76	8.15		12.01	48.06	60	341.1				
CFAT-R10-L8-20	160.49	10.23	4829.13	15400.40	31.36		7.98	31.90	20	1297.2				
CFAT-R10-L8-40	160.20	10.15	4784.67	15371.82	31.13	1280	7.99	31.96	40	962.1	2	252.13	296.17	71901
CFAT-R10-L8-60	159.99	10.02	4720.87	15382.81	30.69		8.00	32.00	60	792.9				
CFAT-R10-L12-20	160.21	10.24	4824.52	15334.48	31.46		11.98	47.94	20	1116.7				
CFAT-R10-L12-40	160.17	10.10	4761.73	15387.20	30.95	1920	11.99	47.95	40	834.7	2	252.13	296.17	71901
CFAT-R10-L12-60	160.04	10.05	4735.63	15380.61	30.79		12.00	47.99	60	639.4				
CFAT-S6.3-L8-20	160.21	6.28	3866.72	21800.52	17.74		7.99	27.68	20	1089.1				
CFAT-S6.3-L8-40	160.22	6.31	3884.69	21785.76	17.83	1280	7.99	27.67	40	948.6	3	212.08	258.46	65044
CFAT-S6.3-L8-60	160.42	6.25	3854.25	21880.33	17.62		7.98	27.64	60	554.6				
CFAT-S6.3-L12-20	160.24	6.26	3855.66	21821.20	17.67		11.98	41.51	20	960.4				
CFAT-S6.3-L12-40	160.39	6.33	3900.80	21824.15	17.87	1920	11.97	41.47	40	815.9	3	212.08	258.46	65044
CFAT-S6.3-L12-60	160.42	6.27	3866.08	21868.49	17.68		11.97	41.46	60	552.6				

In Table 1, failure mode 1 indicates flexure failure, showing that local buckling occurs at the mid-height area of aluminum tube and cracks appear at the tensile area of internal concrete. Failure mode 2 indicates specimen flexure failure occurs, but local buckling does not occur on aluminum tube, while cracks appear at the tensile area of the concrete. Failure mode 3 indicates specimen occurs flexure failure, showing that local buckling occurs at the mid-height area of aluminum tube and cracks appear at the tensile area of internal concrete, while the concrete is crushed in the compression area.

2.2 Mechanical properties of materials

Standard tensile tests were carried out to obtain the material mechanical parameters of aluminum alloy tubes used in this experiment. As cold-formed metal tubes are reinforced during production due to cold working, cooling methods (such as air cooling and water quenching) have an influence on the mechanical properties of 6061 aluminum alloy [36]. For circular aluminum tubes, bent coupons were extracted from random locations within the cross-section, while for square aluminum tubes, coupons were extracted from flat regions [37,38]. Tensile coupons extracted from the circular or square aluminum tubes were differentiated by their section identifier (the letter "R" and "S" respectively represent circular sections and square sections) and the thickness (3 mm, 10 mm, or 6.3 mm). Each coupon was prepared in conformance with GB/T228.1-2010 [39], with a 45 mm parallel width and a gauge length of 260 mm (for 3 mm thick circular tube), 290 mm (for 10 mm thick circular tube) and 270 mm (for square tubes) respectively. It should be noted that although all aluminum alloy tubes in this test are from the same manufacturer, different cooling methods are adopted for aluminum tubes with different sections in the production process. Specifically, circular tubes are cooled by water quenching, while square tubes are cooled by air cooling.

The mechanical parameters of aluminum alloy materials are measured on the UTM5305-G instrument (see Fig. 1) by displacement controlling. The constant displacement rate is 0.015 mm per min, according to the provisions of GB/T228.1-2010 [39]. The strains of tensile coupons were measured by an extensometer YYU-10/50 whose errors of relative standard distance, relative displacement and absolute displacement are respectively less than 0.005, 0.005 and 1.5 μm. The load values were obtained by the sensors inside the instrument.

The typical stress-strain curves of all coupons are plotted in Fig. 3. The measured static 0.2% proof stress $\sigma_{0.2}$ ($f_{0.2}$), static ultimate tensile stress σ_u (f_u), and Young's modulus E_0, are listed in Table 1. As shown in Fig. 3, the curves of the two groups of coupons (R3 and R10) are in good agreement, especially in the values of $\sigma_{0.2}$ and σ_u. On the contrary, the curve of coupon S6.3 shows an obvious difference from that of R3 and R10. It has not only much less values of $\sigma_{0.2}$ and σ_u, but also much little ductility than that of circular tubes. This may be attributed to the influence of cooling methods on the mechanical behaviors of aluminum alloy material [36].

Fig. 1. Test set-up for longitudinal tensile coupons

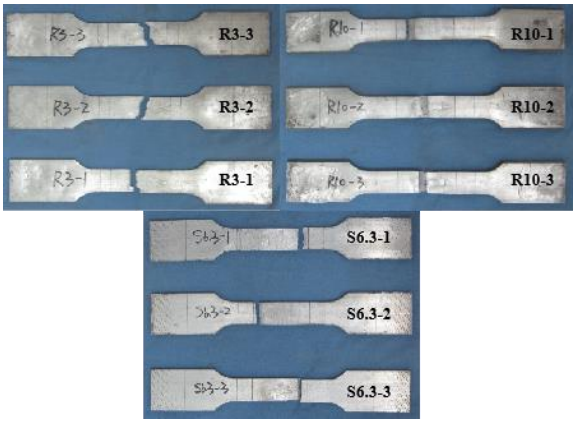

Fig. 2. The failed tensile specimens of 6061-T6 aluminum alloy

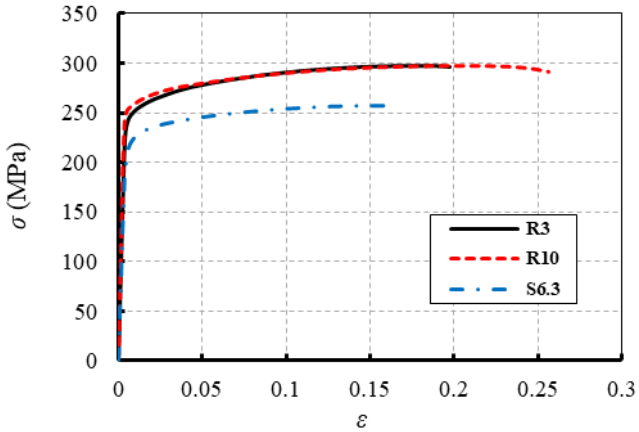

Fig. 3. The stress-strain curves of longitudinal tensile coupon tests

The aluminum tubes were filled with commercial concrete of C30 grade, and the mix proportion is listed in Table 2. Cubes with 150mm side length were cast and then cured together with the CFAT columns [40]. The tested compressive strength of the cubes is 42.9 MPa.

Table 2 Mix proportion of concrete

Material	Type	Consumption (kg/m^3)	Mix proportion
Cement	42.5R-Ordinary Portland Cement	280.0	1.00
Water	water	176.0	0.63
Sand	River sand and artificial sand	802.0	2.86
Stone	Gravel (particle fraction during 5-20)	1063.0	3.80
Mixture	I-Fly ash	79.0	0.28
Admixture	YD-2-Superplasticizer	10.1	0.04

2.3 Application and control of load

The compression tests of columns were conducted using a long-axis servo-controlled testing machine produced by Hangzhou Popwil Instrument Co., Ltd., in combination with a pair of designated support devices, as shown in Fig. 4. The instrument has a maximum loading range of 7000 kN, a loading accuracy of 1.0 N and a displacement accuracy of 0.1 mm. Both ends of the CFAT column were supported by a knife-shaped device, consisting of a wedge plate with a knife-edge wedge and a pit plate with several semi-circle pits, through which the pin-ended supports to the specimen ends were formed. The varying eccentricities were then achieved by matching the wedge with the pit at predefined locations relative to the central lines of the pit plate. Additionally, two profiled steel tubes (100 mm height for circular specimens and 95 mm height for square specimens) were used to strengthen the ends, which was expected to avoid the early failure of the column ends.

In this test, an eccentric force was applied to the top surface of each tested column by displacement controlling method with a rate of 0.5 mm per minute. When the load value decreases to less than 70% of the maximum value or the vertical displacement of the upper loading plate reaches 30 mm, the test was terminated.

2.4 Measurement content and instrument layout

The test set-ups of typical circular and square cross-section CFAT long columns are illustrated in Fig. 4. Four displacement meters (YHD-50) were respectively vertically located at each corner of the upper loading plate to measure the vertical displacement of the top end of the column. Three displacement meters were respectively arranged at the 1/4 height (YHD-100), 1/2 height (YHD-200) and 3/4 height (YHD-100) of the column to measure the corresponding lateral deflections, as displayed in Fig. 5(a). The displacement measurement accuracies of YHD-50, YHD-100 and YHD-200 are all 0.01 mm, while the maximum ranges of them are respectively 50 mm, 100 mm and 200 mm.

Four strain measuring points were arranged at mid-height of each tested column (see Fig.5). There are two strain gauges (BX120-5AA) at each point for respectively measuring the longitudinal strain and hoop strain of the tube.

The data of displacement and strain were recorded by a DH3518 data acquisition instrument produced by Donghua Test Technology Co., Ltd.

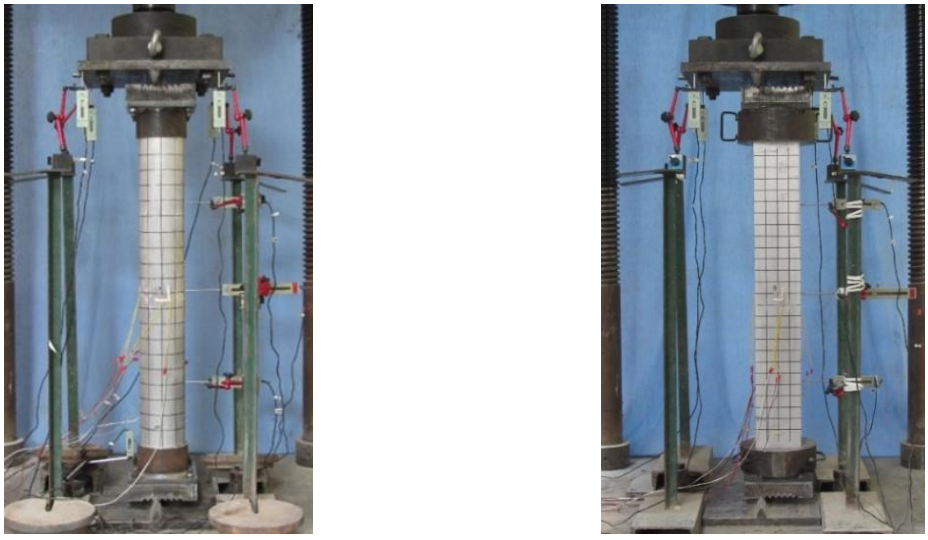

(a) CFAT-R3-L8-20 (b) CFAT-S6.3-L8-60

Fig. 4. Test set-up for CFAT long column specimens

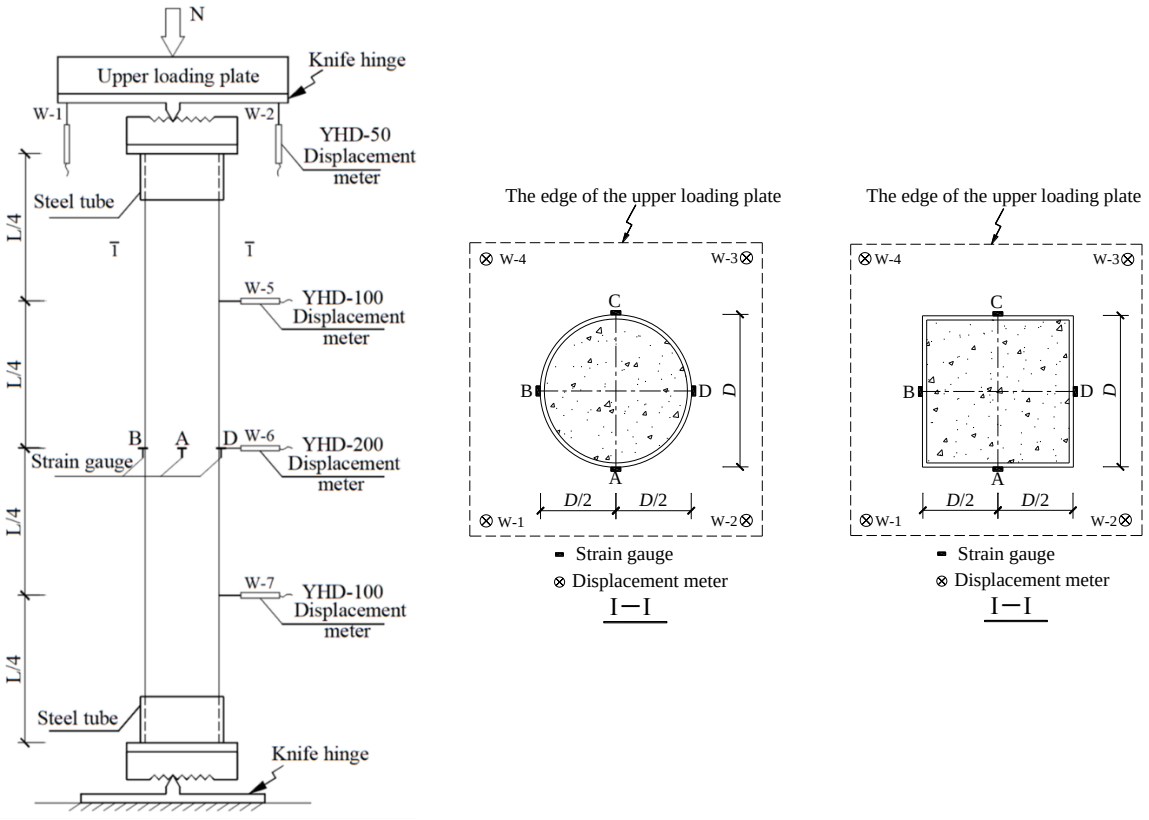

(a) Front view (b) Circular specimens (c) Square specimens

Fig. 5. Test device layout

3 Results and analysis

3.1 Failure modes

Upon testing, the specimens were grouped by their cross-sections and displayed in Fig. 6, showing that all the specimens appeared flexural dominated failure. Failure modes of all tested specimens are summarized in Table 1. The concrete cracks of typical specimens are exposed and displayed in Fig.7. It can be found that those circular specimens with a thickness of 3 mm of the tube (including not only those with an L/D ratio of 8, but also those with an L/D ratio of 12) occurred flexure failure, showing that local buckling occurs at the mid-height area of aluminum tube and cracks appear at the tensile area of internal concrete. All the other circular specimens (with a wall thickness of 10 mm) occurred flexure failure, and local buckling does not appear on the aluminum tube, while cracks appear at the tensile area of the concrete. On the

other side, all the square specimens in this test occurred flexure failure, showing that local buckling occurs at the middle part of the tube and cracks appear at the tensile area of internal concrete, while the concrete is crushed in the compression area.

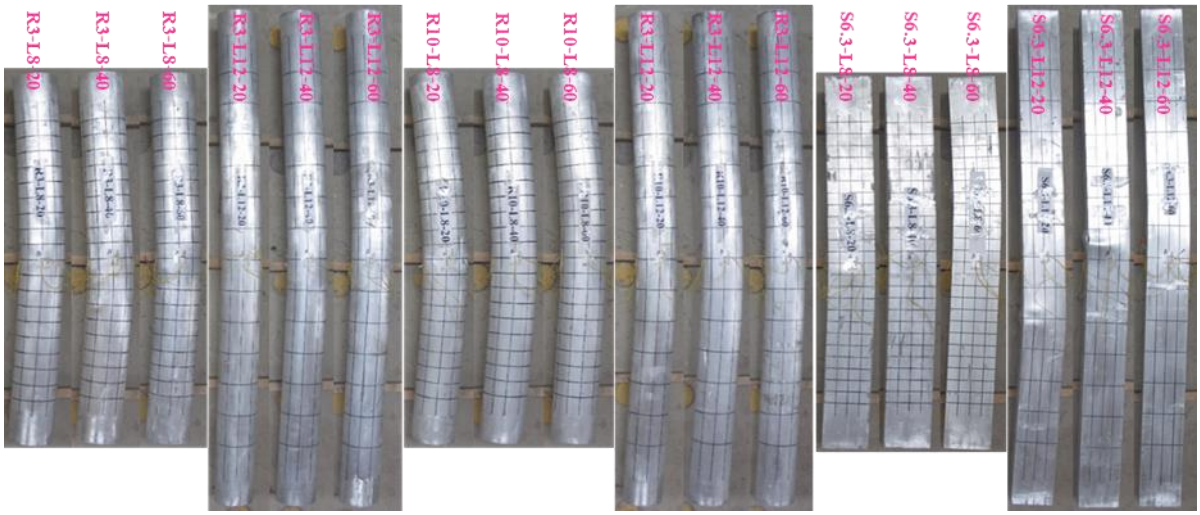

Fig. 6. Summary of failed specimens

It was also found that, within the same group of specimens, the change of eccentricity had no obvious effect on the overall failure modes of CFAT columns. The local buckling degree of the aluminum tube generally increased with the reduction of the slenderness ratio. However, both eccentricity and slenderness ratio had a great impact on the failure of internal concrete. For brevity of this paper, only one specimen of each group was selected to describe and compare the lateral deflection and damage observations of concrete, as shown in Fig. 7. The lateral deflections of the columns at different load levels are presented, and curves are approximately in the shape of half-sine waves (less so for square specimens). The internal concrete of all square specimens was crushed, while that of circular specimens was not crushed owing to a higher crushing strain as a consequence of better confinement afforded by circular shape aluminum tubes. The test results revealed that all the specimens exhibited flexural-dominated failure, and the change of eccentricity had no obvious impact on the overall failure mode of the aluminum

tube while significantly affecting the damage of internal concrete. This indicates that the increase in eccentricity reduced the confinement of aluminum tubes on internal concrete.

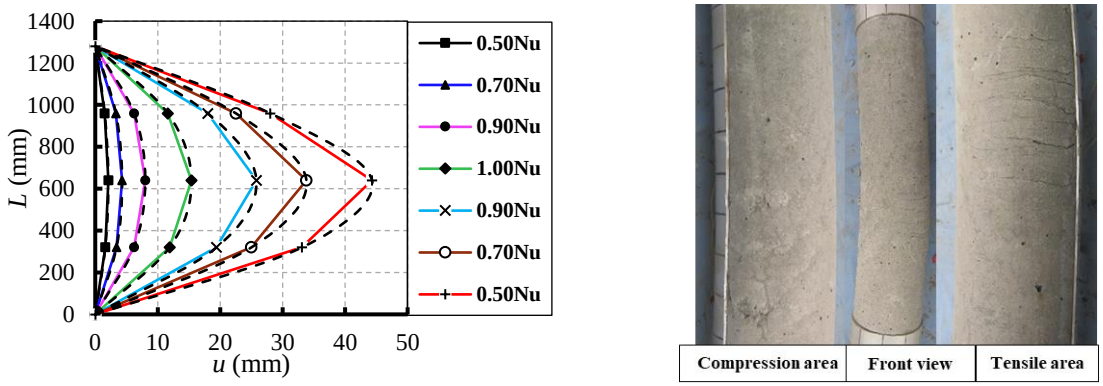

(a) CFAT-R3-L8-40

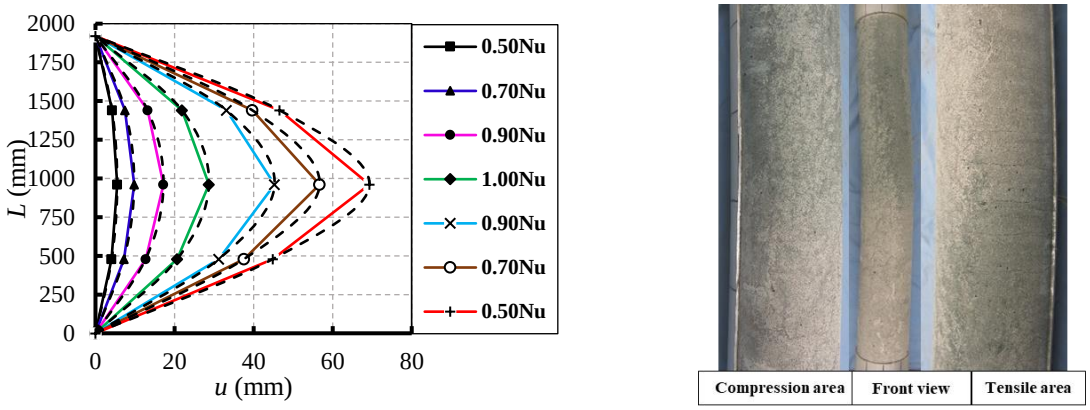

(b) CFAT-R3-L12-40

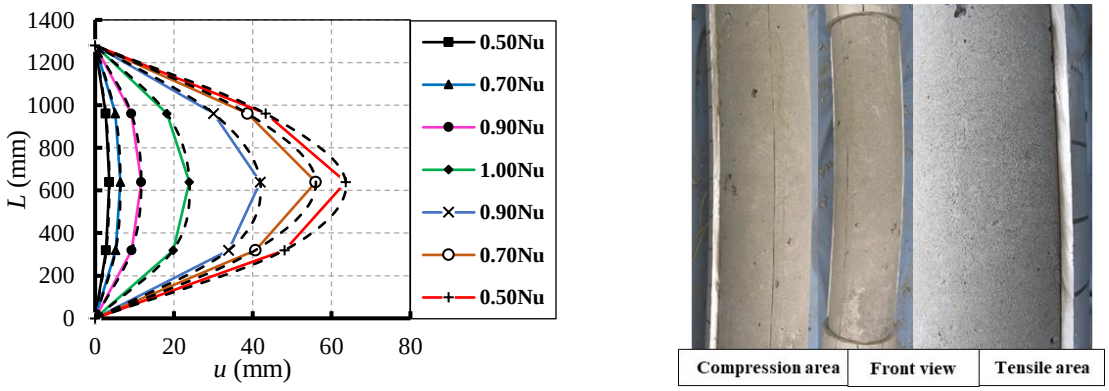

(c) CFAT-R10-L8-40

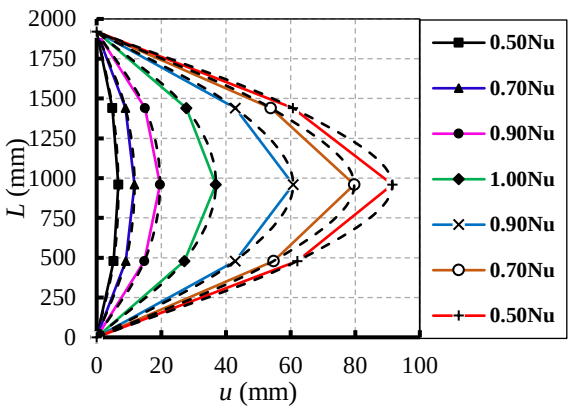

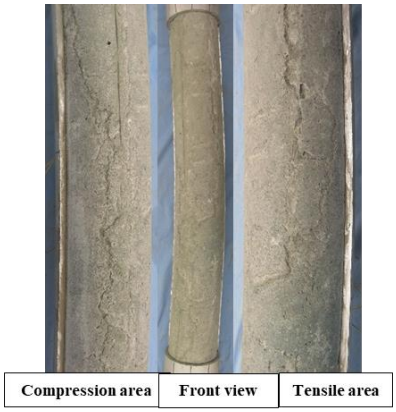

(d) CFAT-R10-L12-40

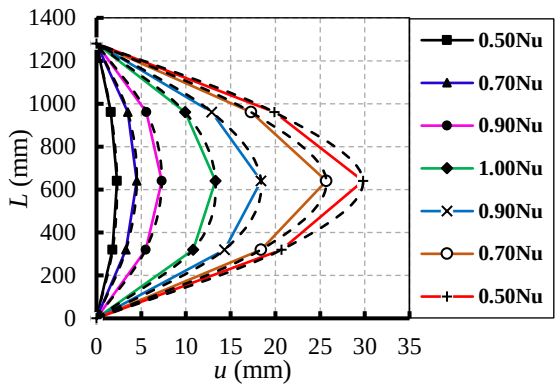

(e) CFAT-S6.3-L8-40

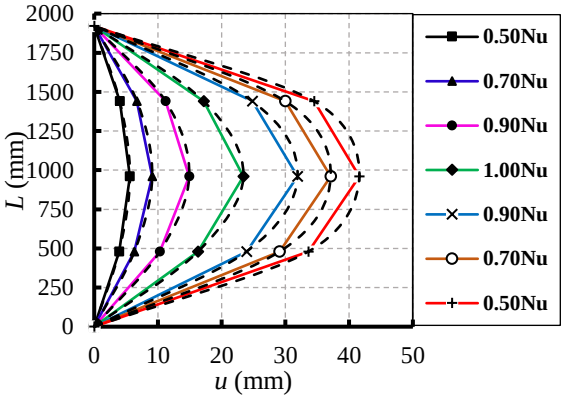

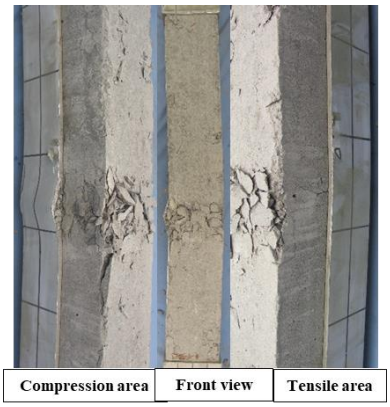

(f) CFAT-S6.3-L12-40

Fig. 7. Lateral deflection along the column at different load levels and corresponding failure mode

3.2 Load-deformation relationship

Fig. 8 shows the load versus mid-height lateral deflection (N-U_m) curves for the eccentric loading CFAT long columns. It can be seen from Fig. 8 (a) that when the eccentricity keeps unchanged, the general trend of N-U_m curves of specimens with different aluminum ratios appeared similar. It was also found that when the aluminum ratio increased from 7.9% to 30.6%,

the mid-height lateral deflection at the ultimate load of specimens increased by 31% ~ 53%, and the initial stiffness also increased by 25~61%. As can be seen from the failure mode of CFAT-S6.3-L12-60 in Fig. 6, the flexural deformation of this specimen did not occur in the mid-span region, thus resulting in a small lateral deflection corresponding to the ultimate load reached. Apart from the specimens CFAT-S6.3-L12-60, it is generally observed that the increase in eccentricity from 20 mm to 60 mm resulted in significant increases in mid-height lateral deflections for the specimens with the same aluminum ratio. With the increase in eccentricity, the initial stiffness decreased while the lateral deformability increased. As shown in Fig. 8 (b) and (c), when the eccentricity kept the same and the slenderness ratio increased from 32 to 48, the mid-height lateral deflection of specimens increased by 57% ~ 88%. With the increase of slenderness ratio, the initial stiffness decreased accompanied by a slight increase in the lateral deformability. It also can be found in Fig. 8 (d) that the lateral deformability of circular CFAT columns was better than that of square columns at the same eccentricity.

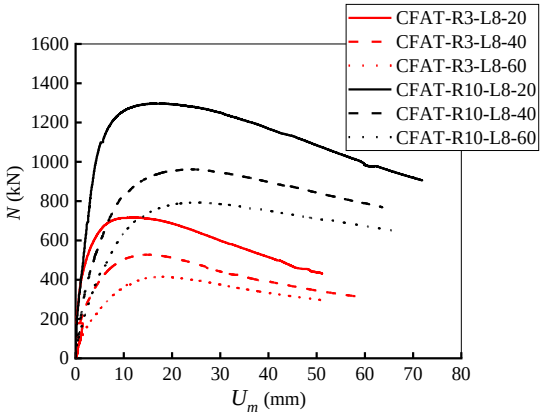

(a)

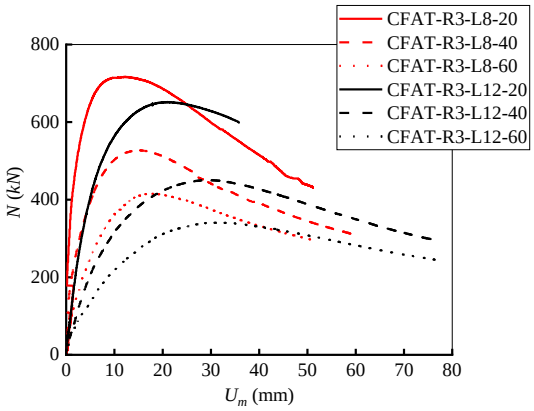

(b)

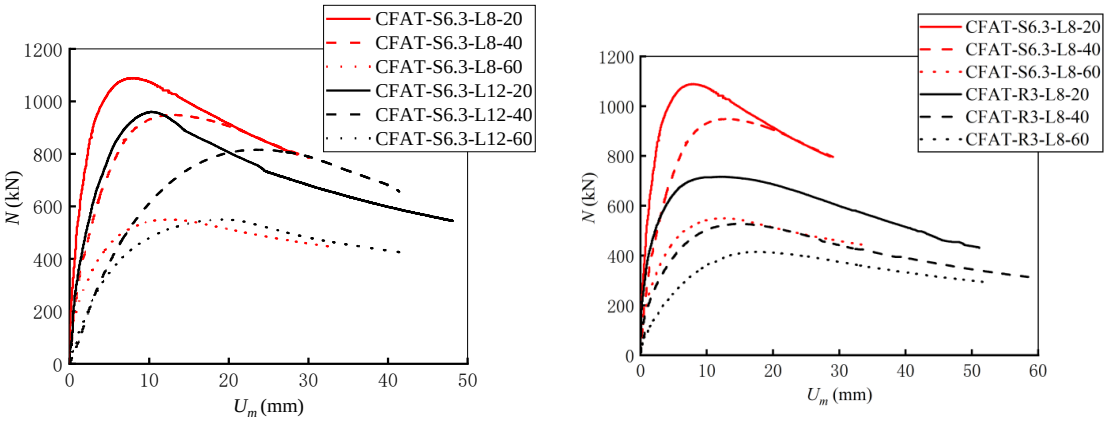

(c) (d)

Fig. 8. Load (N) - lateral deflections (U_m) at mid-heights

3.3 Stress-strain analysis of aluminum tube

The load-longitudinal strain curves and load-hoop strain curves are displayed in Figures 9 and 10 respectively. In these figures, the tensile and compressive yield strains of the aluminum tubes are also displayed vertical dotted lines. The yield strains of each examined aluminum tube are obtained by using the measured yield strengths and Young's modulus. For circular aluminum tubes with a thickness of 3 mm and 10 mm, the yield strains ε_3 and ε_{10} are 5515 and 5506 respectively. For square tubes with a wall thickness of 6.3 mm, the yield strain $\varepsilon_{6.3}$ is 5261.

It can be found from the load-longitudinal strain curves that the aluminum tubes of all specimens yielded at both compression and tensile regions upon testing. For circular and square specimens, the aluminum tubes of all the specimens yielded after reaching the ultimate bearing capacity at the tensile regions, and the tensile strains corresponding to the ultimate bearing capacities increased with an increase in eccentricity, as shown in Fig. 9.

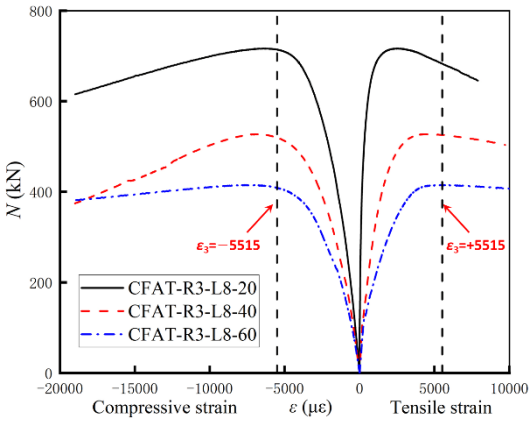

(a) t=3 mm, λ=32

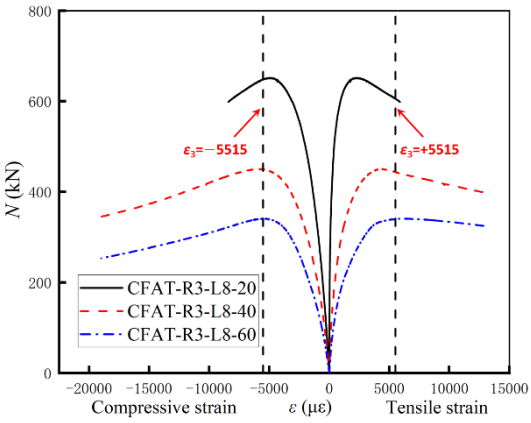

(b) t=3 mm, λ=48

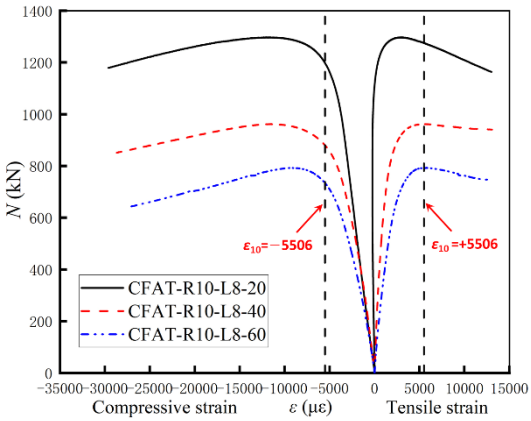

(c) t=10 mm, λ=32

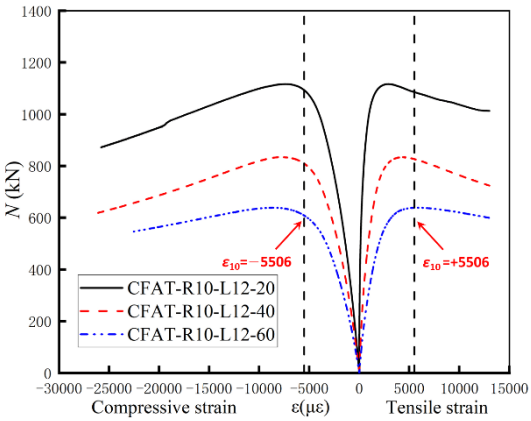

(d) t=10 mm, λ=48

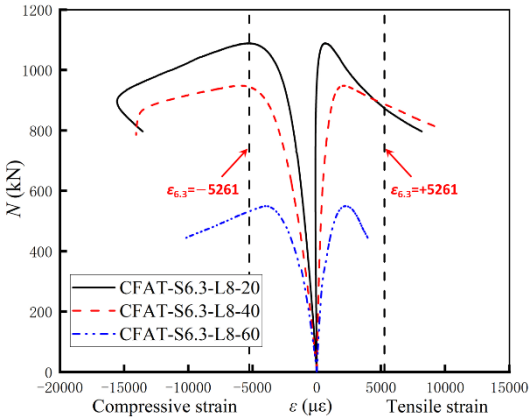

(e) t=6.3 mm, λ=27. 71

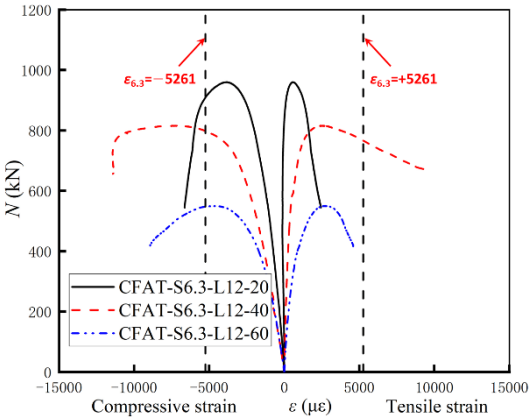

(f) t=6.3 mm, λ=41.57

Fig. 9. Load-Longitudinal strain curves

As shown from the load-hoop strain curves, all of the specimens' tubes yielded at the tensile area upon testing, except for CFAT-S6.3-L12-20. In the compression area, only the

circular tubes with a wall thickness of 10 mm and the specimen with a slenderness ratio of 8 yielded after reaching the ultimate capacities of specimens, indicating that the hoop confinement effect of the aluminum tubes on the internal concrete was not significant when the tube is not thick enough. Through comparisons among specimens with varying slenderness ratios, has little effect on the change of hoop strain. On the whole, the lateral confinement effect of square aluminum tubes on internal concrete is weaker than that of circular aluminum tubes.

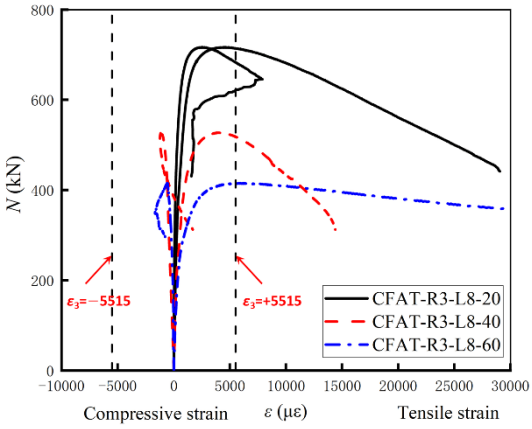

(a) t=3 mm，λ=32

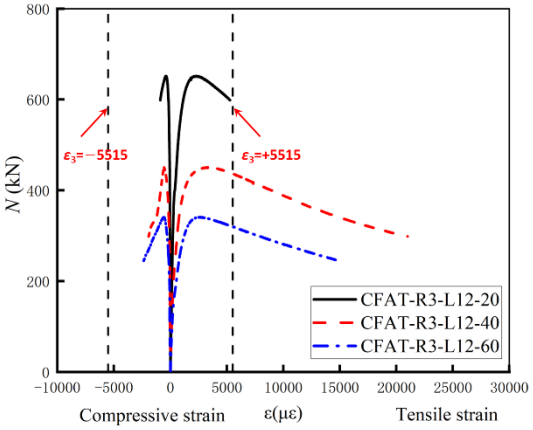

(b) t=3 mm，λ=48

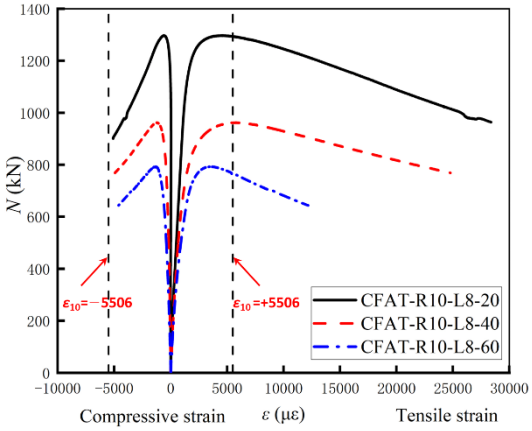

(c) t=10 mm，λ=32

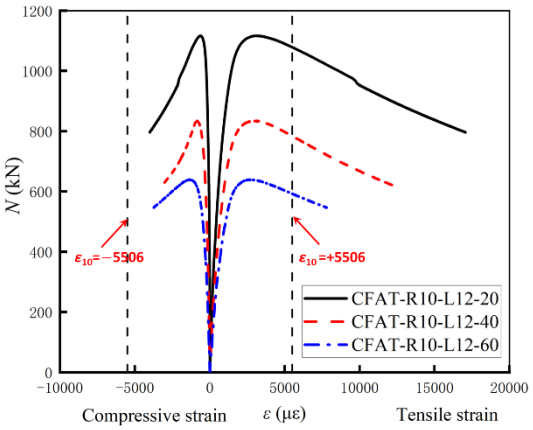

(d) t=10 mm，λ=48

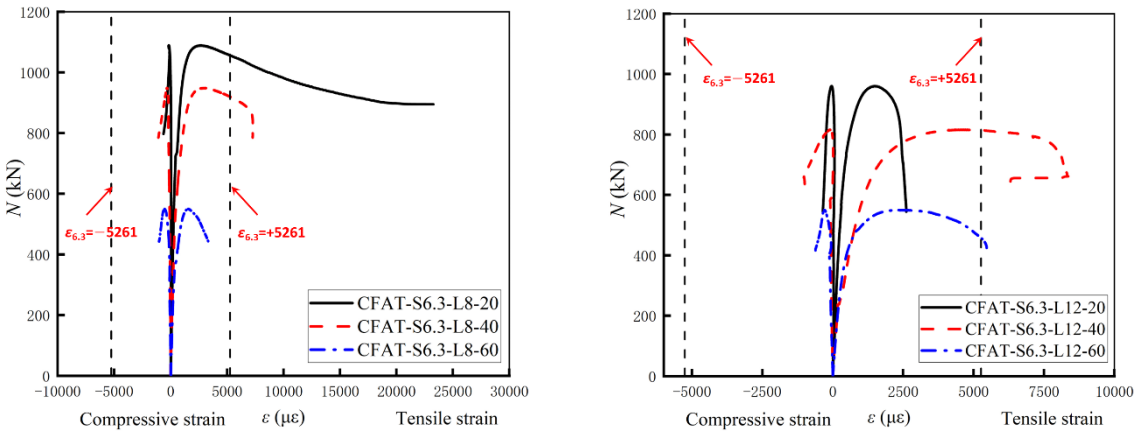

(e) t=6.3 mm，λ=27. 71　　(f) t=6.3 mm，λ=41.57

Fig. 10. Load-hoop strain curves

4 Prediction of the bearing capacities of CFAT

4.1 General

There are still no design provisions to predict the compression capacities of CFAT long columns under eccentric loading. Therefore, in this part, the applicability of current design provisions to the investigated CFAT columns was evaluated. The test bearing capacities were compared with the predicted values of the design resistance of composite carbon steel components determined in the European code EC4 [8] and two Chinese design codes GB 50936-2014 [33] and CECS 28:2012 [35].

4.2 European code EC4

CFAT columns under eccentric compression can be essentially treated as CFAT beam-columns and designed based on interaction curves for combined compression and uniaxial bending. The design provisions provided by EC4 [8] for CFST long columns under eccentric compression are used herein for the predictions of CFAT columns. To facilitate direct comparison and applicability evaluation in this paper, the following modification was made in the calculation: aluminum alloy is used in place of carbon steel for the tube, and hence the yield

stress is replaced by the static 0.2% proof stress $\sigma_{0.2}$ ($f_{0.2}$) measured in this test. The cross-section capacities (N_{EC}) of the tested circular and square CFAT columns are calculated based on the simplified interaction curves (a polygonal diagram) presented in Fig. 11. In Fig. 11, points A and B respectively correspond to the plastic compression resistance (N_{pl}) and moment resistance (M_{pl}) of a column. Point C corresponds to the point where the moment capacity is equal to the plastic capacity and the axial load is equal to N_{pm}. Point D is determined with the neutral axis being the middle of the cross-section and the corresponding moment capacity and axial load are equal to M_{max} and $0.5N_{pm}$.

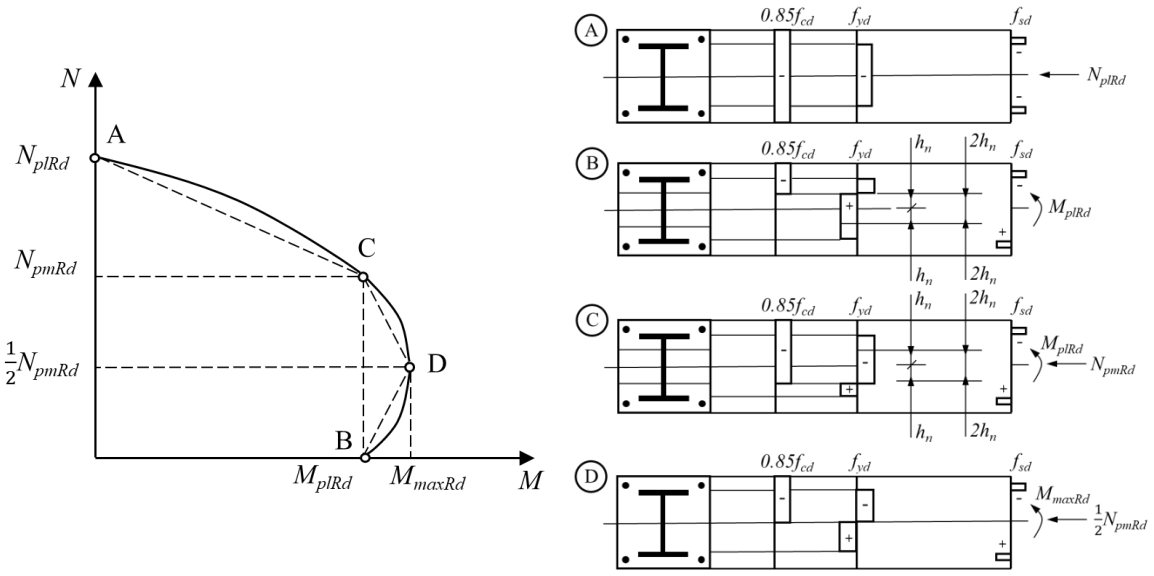

Fig. 11. Simplified interaction curve and corresponding stress distributions in EC4 [8]

The plastic compression resistance N_{pl} of the column can be determined by Eq. (1),

$$N_{pl} = f_c' A_c + f_{0.2} A_a \quad (1)$$

where A_c and A_a are respectively the section area of the internal concrete column and aluminum alloy tube, f_c' is the compression strength of the concrete cylinder, $f_{0.2}$ is the static 0.2% proof stress of aluminum alloy.

The plastic moment resistance is determined by assuming full plastic stress distribution across the whole section, as detailed in [41,42]. The M_{max} is determined when the neutral axis

is in the middle of the cross-section and N_{pm} is essentially equal to the compressive capacity of the whole concrete section area, taken as $A_c f_c'$.

The following expression based on Fig. 11 should be satisfied:

$$\frac{M_{ED}}{M_{plNRd}} = \frac{M_{ED}}{\mu_d M_{plRd}} \le \alpha_M \tag{2}$$

where M_{ED} is the maximum end moment and maximum bending moment within the column length, which includes defects and second-order effects if necessary, and M_{plN} is the plastic bending resistance considering the normal force N_{ED}, given by μM_{pl}, M_{pl} is the plastic bending resistance, given by point B in Fig. 11. The coefficient α_M should be taken as 0.9 for steel grades S235 and S355, and 0.8 for steel grades S420 and S460. In this paper, α_M is taken as 0.9 based on the strength range of aluminum tubes.

The straight line is taken as $M=N(e+\delta)$, where e is the initial eccentricity in the examined column, and δ is the mid-span lateral displacement corresponding to the ultimate bearing capacity of the column, and $e+\delta$ represents the final eccentricity of the column specimen considering the second order effects. The intersection of the straight line and the interaction curve is the final axial capacity N_{EC} and M_{EC}, as is shown in Fig. 12.

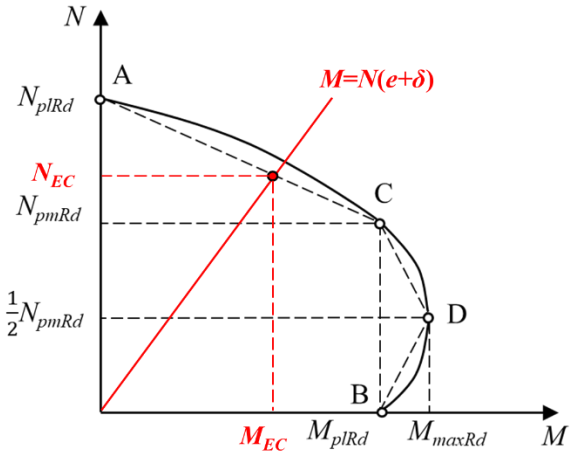

Fig. 12. The calculation of design axial capacity N_{EC} and M_{EC}

4.3 Chinese design provision GB 50936-2014

In Chinese design provision GB 50936-2014 [33] for CFST structures, CFST columns under combined compression and uniaxial bending are designed based on the interaction equation in Eq. (3),

$$\frac{N_{GB}}{N_u}+\frac{M_{GB}}{1.5M_u\left(1-0.4N_{GB}/N_E^{'}\right)}\le 1 \tag{3}$$

where N_{GB} is the ultimate axial load of the column under the eccentric loading condition, M_u is the ultimate moment, N_u is the axial bearing capacity of CFST long columns, and M_u is the ultimate moment capacity of the member, in which $N_E^{'}$ is the critical bearing capacity of CFAT sections and calculated by Eq. (4),

$$N_E^{'}=\frac{\pi^2 E_{ac}A_{ac}}{1.1\lambda^2} \tag{4}$$

Note that N_u is calculated by employing a reduction factor φ, associated with normalized slenderness ratio ($\bar{\lambda}_{ac}$) of the column, to the axial compressive capacity (N_0) of the cross-section, as calculated by Eqs. (5) ~ (10).

$$N_u=\varphi N_0 \tag{5}$$

$$\varphi=\frac{1}{2\bar{\lambda}_{ac}}\left[\bar{\lambda}_{ac}^2+\left(1+0.25\bar{\lambda}_{ac}\right)-\sqrt{\left(\bar{\lambda}_{ac}^2+\left(1+0.25\bar{\lambda}_{ac}\right)\right)^2-4\bar{\lambda}_{ac}^2}\right] \tag{6}$$

$$\bar{\lambda}_{ac}=\frac{\lambda_{ac}}{\pi}\sqrt{\frac{f_{ac}}{E_{ac}}}\approx 0.01\lambda_{ac}\left(0.001f_{0.2}+0.781\right) \tag{7}$$

$$N_0=A_{ac}f_{ac} \tag{8}$$

$$f_{ac}=\left(1.212+B\theta+C\theta^2\right)f_c \tag{9}$$

$$\theta=\frac{A_a f_{0.2}}{A_c f_{0.2}} \tag{10}$$

Here, E_{ac} is the combined elastic modulus of CFAT sections. f_{ac} is the compression strength of a CFAT section, determined by Eq. (9). θ is the coefficients of confinement effect, determined

by Eq. (10). f_c is the compression strength of the concrete prism. B and C are coefficients of influence of section shape on hoop effect, as given by Eqs. (11) and (12). A_{ac} is the total section area of the column.

$$B=\begin{cases}0.176\,f_{0.2}/213+0.974 & \text{for circular section}\\ 0.131\,f_{0.2}/213+0.723 & \text{for square section}\end{cases} \tag{11}$$

$$C=\begin{cases}-0.104\,f_c/14.4+0.031 & \text{for circular section}\\ -0.070\,f_c/14.4+0.026 & \text{for square section}\end{cases} \tag{12}$$

The ultimate moment capacity (M_u) is given as $\gamma_m W_{ac} f_{ac}$, in which W_{ac} is the modulus of the combined section of the flexural member, and γ_m is the plastic development coefficient.

4.4 Chinese design provision CECS 28:2012

In Chinese design provision CECS 28:2012 [35] for CFST structures, CFST columns under eccentric compression are designed by employing reduction factors φ_e and φ_l associated with eccentricity and slenderness ratio, as calculated by Eqs. (13) ~ (15).

$$N_{CE}=\varphi_l\varphi_e N_0 \tag{13}$$

where φ_e and φ_l are the reduction factors associated with eccentricity and slenderness ratio respectively, which are determined by Eqs (14) and (15), respectively. In Eqs (14) and (15), r_c is the radius of the concrete section. L is the length of CFAT columns. D is the diameter for circular CFAT columns or the width (depth) for square CFAT columns. N_0 is the axial bearing capacity of a CFAT stub column, as determined in Eq. (16), in which the coefficient α should be taken as 2.0 for concrete below C50 or 1.8 for concrete beyond C55. θ is the coefficient of confinement effect, as given by Eq. (17).

$$\varphi_e=\begin{cases}\dfrac{1}{1+1.85e/r_c} & e/r_c\le 1.55\\ \dfrac{0.4}{e/r_c} & e/r_c>1.55\end{cases} \tag{14}$$

$$\varphi_l = \begin{cases} 1 - 0.115\sqrt{L/D - 4} & L/D > 4 \\ 1 & L/D \le 4 \end{cases} \tag{15}$$

$$N_0 = \begin{cases} 0.9A_c f_c (1 + \alpha\theta) & 0.5 < \theta \le 1 \\ 0.9A_c f_c \left(1 + \sqrt{\theta} + \theta\right) & 2.5 > \theta > 1 \end{cases} \tag{16}$$

$$\theta = \frac{A_a f_{0.2}}{A_c f_{0.2}} \tag{17}$$

Table 3 Comparison of predicted capacities with test results for circular CFAT long columns

Specimen	N_{ue}	GB [33]		CECS [35]		EC4 [8]	
		N_{GB}	N_{GB}/N_{ue}	N_{CE}	N_{CE}/N_{ue}	N_{EC}	N_{EC}/N_{ue}
R3-L8-20	716.6	683.7	0.954	640.0	0.893	670.23	0.935
R3-L8-40	527.5	515.2	0.977	489.6	0.928	634.20	1.202
R3-L8-60	415.4	406.0	0.977	387.4	0.933	603.06	1.452
R3-L12-20	652.0	590.4	0.906	561.3	0.861	630.82	0.968
R3-L12-40	450.8	449.5	0.997	427.9	0.949	584.72	1.297
R3-L12-60	341.1	362.5	1.063	340.0	0.997	554.76	1.626
R10-L8-20	1297.2	1203.8	0.928	1183.6	0.912	1074.40	0.828
R10-L8-40	962.1	945.7	0.983	891.9	0.927	941.86	0.979
R10-L8-60	792.9	783.8	0.989	715.5	0.902	863.73	1.089
R10-L12-20	1116.7	1030.7	0.923	1033.9	0.926	933.10	0.836
R10-L12-40	834.7	815.7	0.977	779.9	0.934	828.04	0.992
R10-L12-60	639.4	685.3	1.072	626.1	0.979	743.40	1.163
Mean			0.979		0.928		1.114
Standard			0.048		0.035		0.246
COV			0.049		0.037		0.221

Table 4 Comparison of predicted capacities with test results for square CFAT long columns

Specimen	N_{ue}	GB [33]		CECS [35]		EC4 [8]	
		N_{GB}	N_{GB}/N_{ue}	N_{CE}	N_{CE}/N_{ue}	N_{EC}	N_{EC}/N_{ue}
S6.3-L8-20	1089.1	1130.2	1.038	1073.3	0.985	823.26	0.756
S6.3-L8-40	948.6	906.4	0.956	817.0	0.861	741.79	0.782
S6.3-L8-60*	554.6	741.7	1.337	652.4	1.176	691.17	1.246
S6.3-L12-20	960.4	1016.6	1.059	938.4	0.977	775.52	0.807
S6.3-L12-40	815.9	813.2	0.997	712.8	0.874	672.18	0.824
S6.3-L12-60*	552.6	682.1	1.234	572.0	1.035	635.16	1.149
Mean			1.012		0.924		0.927
Standard			0.040		0.057		0.213
COV			0.039		0.062		0.230

4.5 Discussion and design recommendations

The comparison of test bearing capacities (N_{ue}) with predicted bearing capacities (Code EN 1994-1-1 (EC4) [8], GB 50936-2014 [33], and CECS 28:2012 [35]) is respectively

illustrated in Table 3 and Table 4 for the investigated circular and square CFAT long columns. For the GB 50936-2014 [33], the mean value of the N_{GB}/N_{ue} ratio is 0.979 with the corresponding coefficient of variation (COV) of 0.049 for the circular CFAT long columns, as shown in Table 3, indicating a high degree of accuracy and consistency. The predictions from GB 50936-2014 [33] for the square CFAT long columns are also in good agreement with the test results, achieving a mean value of the N_{GB}/N_{ue} ratio of 1.012 with the corresponding COV of 0.039, as shown in Table 4. Compared to GB 50936-2014 [33], CECS 28:2012 provided slightly more conservative yet consistent predictions for both circular and square CFAT long columns. However, Eurocode EN 1994-1-1 (EC4) [8] resulted in some unsafe predictions for circular CFAT long columns, particularly for specimens with large eccentricities. The mean value of the N_{EC}/N_{ue} ratio is 1.114 with the corresponding COV of 0.221 for the circular CFAT long columns, as shown in Table 3. For square CFAT long columns, design predictions from EC4 were generally very conservative for specimens with small eccentricities while rather unsafe for specimens with large eccentricities, as shown in Table 4. Overall, it can be concluded that, for both circular and square specimens, GB 50936-2014 [33] and CECS 28:2012 [35] yielded accurate predictions with a great level of consistency and thus recommended for the design of circular and square CFAT long column under eccentric compression.

5 Conclusions

In this paper, an experimental investigation of the eccentric compression behaviors of CFAT long columns was carried out. The main conclusions are as follows.

(1) All specimens exhibited flexural-dominated failure. The variation of eccentricity has no apparent influence on the aluminum tube's overall failure mode, while it dramatically influences

the failure mode of the internal concrete.

(2) The internal concrete failed in crushing for all square specimens, while remaining intact for circular specimens. This indicates that the circular tube can provide a better confining effect to the internal concrete than the square tube, which leads to a higher compressive bearing capacity of the internal concrete.

(3) It was also found that the increase in eccentricity reduces the hoop confinement effect of aluminum tube on internal concrete, while the slenderness ratio has no obvious impact on the change of hoop strain. On the whole, the lateral confinement effect on internal concrete of the square aluminum tubes is weaker than that of circular aluminum tubes.

(4) The applicability of existing design provisions for CFST long columns to CFAT long columns was evaluated. It is revealed that GB 50936-2014 and CECS 28:2012 yielded accurate predictions with a great level of consistency and thus recommended for the design of CFAT long columns under eccentric compression.

Acknowledgement

This research was supported by the Fundamental Research Funds for the Central Universities (Project number:2019XKQYMS44). The authors gratefully appreciate this support.

Nomenclature

N —Axial pressure acting on member (N)

M —Bending moment acting on member ($N{\cdot}mm$)

N_u —Design value of bearing capacity of member under axial compression (N)

M_u —Design value of compressive bearing capacity of member ($N{\cdot}mm$)

e —Eccentricity in the examined column (mm)

f_c' —Compression strength of the concrete cylinder (MPa)

$f_{0.2}$ —Static 0.2% proof stress of aluminum alloy (*MPa*)

A_c —Cross-sectional area of internal concrete (mm^2)

A_c —Cross-sectional area of aluminum alloy tube (mm^2)

N'_E —Critical bearing capacity of CFAT sections (*N*)

$\overline{\lambda}_{ac}$ —Normalized slenderness ratio of columns

E_{ac} — Combined elastic modulus of CFAT sections (*MPa*)

f_{ac} —Compressive strength of CFAT sections (*MPa*)

θ —Coefficient of confinement effect

B 、C —Coefficient of influence of section shape on hoop effect

A_{ac} —Total section area of members (*mm*)

W_{sc}—Modulus of combined section of flexural member (mm^3)

γ_m—Plastic development coefficient

φ_e—Reduction factors associated with eccentricity

φ_l—Reduction factors associated with slenderness ratio

N_0 — Axial bearing capacity of CFAT stub columns (*N*)

r_c —Radius of the concrete section (*mm*)

D—Diameter for the circular CFAT or the width (depth) for square CFAT specimens (*mm*)

L — Member length of CFAT specimens (*mm*)

f_c —Compression strength of the concrete prism (*MPa*)

References

[1] Pickett J M. Aluminum applications for highway bridges. Journal of the Struct Div 1957;83(4): 83:1-7.

[2] Nakai M, Eto T. New aspects of development of high strength aluminum alloys for aerospace applications. Mat Sci Eng A-Struct 2000;7.

[3] Han L-H, Li W, Bjorhovde R. Developments and advanced applications of concrete-filled steel tubular (CFST) structures: Members. J Constr Steel Res 2014;100:211–28.

https://doi.org/10.1016/j.jcsr.2014.04.016.

[4] Cederwall K, Engstrom B, Grauers M. High-strength concrete used in composite columns. Aci Special Publication 1997.

[5] Zeghiche J, Chaoui K. An experimental behaviour of concrete-filled steel tubular columns. J Constr Steel Res 2005;61(1):53-66.

[6] J.M. Portolés, Romero M L, Filippou F C, et al. Simulation and design recommendations of eccentrically loaded slender concrete-filled tubular columns. Eng Struct 2011;33(5): 1576-1593.

[7] Ehab Ellobody, Mariam F. Experimental investigation of eccentrically loaded fibre reinforced concrete-filled stainless steel tubular columns. J Constr Steel Res 2012;76.

[8] Eurocode 4. Design of composite steel and concrete structures, Part 1.1: General rules and rules for buildings. European Committee for Standarization, Brussels, Belgium, 2004.

[9] Yan B, Zhou X-H, Liu J. Behavior of circular tubed steel-reinforced-concrete slender columns under eccentric compression. J Constr Steel Res 2019;155.

[10] Gopal SR, Manoharan PD. Experimental behaviour of eccentrically loaded slender circular hollow steel columns in-filled with fibre reinforced concrete. J Constr Steel Res 2006;62:513–20. https://doi.org/10.1016/j.jcsr.2005.09.004.

[11] Portolés JM, Romero ML, Bonet JL, Filippou FC. Experimental study of high strength concrete-filled circular tubular columns under eccentric loading. J Constr Steel Res 2011;67:623–33. https://doi.org/10.1016/j.jcsr.2010.11.017.

[12] U. M. S, S. A. J. Axial compression behaviour of long concrete filled double skinned steel tubular columns. Struct 2017;9:157–64. https://doi.org/10.1016/j.istruc.2016.12.002.

[13] Han L-H, Huang H, Zhao X-L. Analytical behaviour of concrete-filled double skin steel tubular (CFDST) beam-columns under cyclic loading. Thin-Walled Struct 2009;47:668–80. https://doi.org/10.1016/j.tws.2008.11.008.

[14] Romero ML, Ibañez C, Espinos A, Portolés JM, Hospitaler A. Influence of ultra-high strength concrete on circular concrete-filled dual steel columns. Struct 2017;9:13–20 https://doi.org/10.1016/j.istruc.2016.07.001.

[15] Ouyang Y, Kwan AKH, Lo SH, Ho JCM. Finite element analysis of concrete-filled steel tube (CFST) columns with circular sections under eccentric load. Eng Struct 2017;148:387–98. https://doi.org/10.1016/j.engstruct.2017.06.064.

[16] Neogi PK, Sen HK, Chapman JC. Concrete-filled tubular steel columns under eccentric loading. J Struct Eng 1969;47(5):187–95.

[17] Kilpatrick A E, Rangan B V. Tests on high-strength concrete-filled steel tubular columns. Aci Struct J 1999;96(2):268-274.

[18] O'Shea M D, Bridge R Q. Design of circular thin-walled concrete filled steel tubes. J Struct Eng 2000; 126(11):1295-1303.

[19] Xue J-Q, Briseghella B, Chen B-C. Effects of debonding on circular CFST stub columns. J Constr Steel Res 2012;69:64–76. https://doi.org/10.1016/j.jcsr.2011.08.002.

[20] Li G-C, Chen B-W, Yang Z-J, Liu Y-P, Feng Y-H. Experimental and numerical behavior of eccentrically loaded square concrete-filled steel tubular long columns made of high-strength steel and concrete. Thin-Walled Struct 2021;159:107289. https://doi.org/10.1016/j.tws.2020.107289.

[21] Uy B, Tao Z, Han L-H. Behaviour of short and slender concrete-filled stainless steel tubular

columns. J Constr Steel Res 2011;67:360–78. https://doi.org/10.1016/j.jcsr.2010.10.004.

[22] Yan X-F, Hassanein MF, Wang F, He M-N. Behaviour and design of high-strength concrete-filled rectangular ferritic stainless steel tubular (CFFSST) short columns subjected to axial compression. Eng Struct 2021;242:112611.

[23] Ahmed M, Tran V-L, Ci J, Yan X-F, Wang F. Computational analysis of axially loaded thin-walled rectangular concrete-filled stainless steel tubular short columns incorporating local buckling effects. Struct 2021;34:4652-68.

[24] Al-Mekhlafi GM, Al-Osta MA, Sharif AM. Behavior of eccentrically loaded concrete-filled stainless steel tubular stub columns confined by CFRP composites. Eng Struct 2020;205:110113. https://doi.org/10.1016/j.engstruct.2019.110113.

[25] He A, Wang F, Zhao O. Experimental and numerical studies of concrete-filled high-chromium stainless steel tube (CFHSST) stub columns. Thin-Walled Structures. 2019;144:106273. https://doi.org/10.1016/j.tws.2019.106273.

[26] Cao B, Zhu L, Jiang X, Wang C. An investigation of compression bearing capacity of concrete-filled rectangular stainless steel tubular columns under axial load and eccentric axial load. Sustainability-Basel 2022;14:8946. https://doi.org/10.3390/su14148946.

[27] Li M, Chen Y, Qian R. Experimental research on the stability parameters of aluminum pipes under axial compression load. Spatial Structures 2000(1): 1-9.

[28] Guo X, Shen Z, Li Y. Theoretical and experimental research on aluminum alloy members under eccentric compression. J Build Struct 2007;28(06): 118-128.

[29] Zhou F, Young B. Tests of concrete-filled aluminum stub columns. Thin-Walled Struct 2008;46(6): 573-583. https://doi.org/10.1016/j.tws.2008.01.003.

[30] Zhou F, Young B. Concrete-filled aluminum circular hollow section column tests. Thin-Walled Struct 2009;47(11): 1272-1280. https://doi.org/10.1016/j.tws.2009.03.014.

[31] Li X, Xing G, Zhang P, Zhang G. Bearing capacity calculation of concrete- aluminum tubular column under axial compression with 7075-high-strength aluminum alloy. Industrial Building 2021;1-9.

[32] Technical specification for concrete-filled steel tubular structures: DBJ/T13-51-2010. Fujian Provincial Department of housing and urban rural development, Fuzhou, 2010 (in Chinese).

[33] Technical code for concrete filled steel tubular structures: GB 50936-2014. Ministry of Housing and Urban-Rural Development of the people's Republic of China, Beijing, 2014. (in Chinese).

[34] Ding F-X, Liao C-B, Wang E, Lyu F, Xu Y-L, Liu Y-C, Feng Y, Shang Z-H. Numerical investigation of the composite action of axially compressed concrete-filled circular aluminum alloy tubular stub columns. Mater R 2021;14(9):2435.

[35] Technical specification for concrete-filled steel tubular structures: CECS 28:2012. China Engineering Construction Standardization Association, Beijing, 2012 (in Chinese).

[36] Ding F-J, Jia X-D, Hong T-J, Xu Y-L, Hu Z. Influence of different heat treatment processes on plasticity and hardness of 6061 aluminum alloy. Mater R 2021;35(8):9.

[37] Huang Y, Young B. The art of coupon tests. J Constr Steel Res 2014;96:159–75. https://doi.org/10.1016/j.jcsr.2014.01.010.

[38] Wang F, Liang Y, Zhao O, Young B. Pin-ended press-braked S960 ultra-high strength steel angle section columns: Testing, numerical modelling and design. Eng Struct

2021;228:111418. https://doi.org/10.1016/j.engstruct.2020.111418.

[39] Metallic materials: Tensile tests - Part 1: Test method at room temperature: GB/T2281-2010. Beijing: Standards Press of China, 2010 (in Chinese).

[40] Standard test method for physical and mechanical properties of concrete: GB/T 50081-2019. Ministry of Housing and Urban-Rural Development of the people's Republic of China, Beijing, 2019. (in Chinese).

[41] Wang F, Young B, Gardner L. Testing and numerical modelling of circular CFDST cross-sections with stainless steel outer tubes in bending. Eng Struct 2021;247:113170.1

[42] Wang F, Young B, Gardner L. Testing, numerical analysis and design of CFDST cross-sections with square stainless steel outer tubes in bending. Journal of Constructional Steel Research. 2023;211:108125.